Original article

The β-carboline analogs as a potent inhibitor for Alzheimer's Disease, molecular docking and dynamics simulation study

Muhammad Taha [a,*], Fazal Rahim [b], Azmat Ali Khan [c,*], Bushra Adalat [b], Syahrul Imran [d,e], Jamilah M. Alshehri [c], Asrar Ahmad [f], Khalid Mohammed Khan [g], Syed Adnan Ali Shah [e,h], Nizam Uddin [i]

[a] Department of Clinical Pharmacy, Institute for Research and Medical Consultations (IRMC), Imam Abdulrahman Bin Faisal University, P.O. Box 31441, Dammam, Saudi Arabia
[b] Department of Chemistry, Hazara University, Mansehra 21300, Khyber Pakhtunkhwa, Pakistan
[c] Pharmaceutical Biotechnology Laboratory, Department of Pharmaceutical Chemistry, Collège of Pharmacy, King Saud University, Riyadh 11451, Saudi Arabia
[d] Faculty of Applied Science, Universiti Teknologi MARA (UiTM), 40450 Shah Alam, Selangor, Malaysia
[e] Atta-ur-Rahman Institute for Natural Product Discovery (AuRIns), Universiti Teknologi MARA Cawangan Selangor Kampus Puncak Alam, Bandar Puncak Alam, Selangor 42300, Malaysia
[f] Center for Sickle Cell Disease, College of Medicine, Howard University, Washington, DC, USA
[g] H.E.J. Research Institute of Chemistry, International Center for Chemical and Biological Sciences, University of Karachi, Karachi, Pakistan
[h] Faculty of Pharmacy, Universiti Teknologi MARA Cawangan Selangor Kampus Puncak Alam, Bandar Puncak Alam, Selangor 42300, Malaysia
[i] Department of Chemistry, University of Karachi, Karachi 75270, Pakistan

ARTICLE INFO

ABSTRACT

The β-carboline scaffold are very potent for encouraging molecular interactions with a wide range of Alzheimer's target. Based on biological importance of carboline nucleus, we have designed a new series of carboline derivatives and screened them for acetyl cholinesterase and butyrylcholinesterase inhibition. The structural interpretation of the synthesized analogs was done by spectroscopic techniques such as ^{1}H NMR, ^{13}C NMR. Almost all analogs of the series exhibited good to moderate inhibition activities. The most potent analog among the series was analog **2** having, three hydroxyl groups on the phenyl ring. The IC$_{50}$ values for this analog was 0.10 ± 0.01 for acetylcholinesterase and 0.30 ± 0.01 for butyrylcholinesterase. To understand the interactions of this analogs with the active sites of enzyme docking study was also carried out.

1. Introduction

Currently there are about 50 million Alzheimer's disease patients, and it is expected that this number will increase up to 150 million by 2050 (Breijyeh and Karaman, 2020). Alzheimer's disease has been professed as global health priority by WHO as there is no everlasting treatment for it (Downer et al., 2021). It is a widespread neuro-deteriorating disease, characterized by memory weakening at the beginning followed by perceptive dysfunction such as visual perception aberrations, decision making and language problems (Huang et al., 2020). Alzheimer's disease mainly affects the hippocampus and neocortex, a region in the temporal lobe that is responsible for learning, memory and natural ability to retain body posture (Boccia et al., 2019; Eichenbaum, 2017). Cholinesterase that belongs to the carboxylesterases is present consistently in high level organisms and is crucial for neurotransmission.

Human cholinesterase is of two types of Acetylcholinesterase (AChE; EC 3.1.1.7) and butyrylcholinesterase (BuChE); (EC 3.1.1.8) (Obaid et al., 2022). Acetylcholinesterase (AChE) a member of the hydrolase superfamily converts acetylcholine into acetate and choline (Obaid et al., 2022). It is mainly present in primary cleft post junctional fold, but its great proportion is present in basal lamina. The major role of AChE is to terminate neuronal transmission and signaling between synapses to prevent AChE dispersal and activation of nearby receptors (Heo et al., 2020).

BuChE is another closely related enzyme to AChE which also plays an effective role in the hydrolysis of acetyl choline. Research have shown that as the Alzheimer's disease progress there is increase in BChE activity in most affected area of brain. This

* Corresponding authors.
  E-mail addresses: mtaha@iau.edu.sa, taha_hej@yahoo.com (M. Taha), azkhan@ksu.edu.sa (A.A. Khan).
Peer review under responsibility of King Saud University.

increase in BuChE plays a crucial role in β-amyloid aggregation during the early stage of senile plaque formation (Mascarenhas et al., 2021). In the advanced stage of Alzheimer's disease when the cholinergic neurons have been destroyed, the amount of AChE decreases while the level of BuChE increases making it the leading Ach metabolic enzyme (Mushtaq et al., 2014). The ACh's duration of action is prolonged by cholinesterase inhibitors, whereby reducing the clinical signs of dementia brought on by the loss of cholinergic neurons or a reduction in cholinergic activity in the brain (Kandiah et al., 2017). Among the drugs that are used for the treatment of minor to severe Alzheimer's disease, rivastigmine is now approved by the U.S. Food and Drug Administration (FDA) which is a dual inhibitor of both AChE and BChE. While galantamine and donepezil are selective inhibitors of AChE only. Therefore, the development of innovative dual inhibitors is important to expand the therapeutic choices and enhance the management of this disorder (Khoury et al., 2018; Wu et al., 2020).

β-carboline is a heterocyclic compound which belongs to alkaloid family. It is also known as nor-harmane, a member of the indole alkaloids family with a pyridine ring attached to an indole molecule (Torromino et al., 2021). They are classified based on saturation and unsaturation of pyridine ring. Unsaturated carboline are designated as aromatic carboline while partially or completely saturated are dihydrocarboline or tetrahydrocarboline (Gooyit et al., 2015; Laine et al., 2014). As a result, synthesized and natural -carbolines were most frequently used for their wide range of biological activities such as anticancer (Aaghaz et al., 2021; Ahmad et al., 2020), anti-malarial (Kamboj et al., 2021; Mathew et al., 2022), anti-viral (Beus et al., 2022; Hegazy et al., 2023), anti-diabetic (Singh et al., 2019; Zhu et al., 2021) and antioxidant (Kontham et al., 2021).

Our research group has reported various indole derivatives as potential inhibitor of Alzheimer's disease and has found promising results (Khan et al., 2023; Taha et al., 2021a, 2021b). Similarly, compounds having hydrazides scaffold are also important compounds due to the presence of azomethine group accompanying the carbonyl group which accounts for various biological activities such as anti-inflammatory (Salgın-Gökşen et al., 2007), antioxidant (Settypalli et al., 2019), anti-cancer (Nasr et al., 2014) and anti-viral (Şenkardeş et al., 2016). Keeping in view the biological significance of indole and hydrazides derivatives, we also synthesized β-carboline hydrazides as potent class of acetylcholinesterase and butyrylcholinesterase inhibitor.

2. Result and discussion

2.1. Chemistry

The methyl 9H-pyrido[3,4-b]indole-3-carboxylate (**I**) was refluxed with mixture of hydrazine hydrate and methanol to form 9H-pyrido[3,4-b]indole-3-carbohydrazide (**II**) 4 h. The 9H-pyrido[3,4-b]indole-3-carbohydrazide (**II**) was treated with various aryl aldehyde along with catalytic amount of acetic acid for 3–4 h to obtain (E)-N'-aryl-9H-pyrido[3,4-b]indole-3-carbohydrazide (**1–16**). The completion of reaction was monitored by TLC and after completion of reaction the solvent was evaporated and obtained crude product was washed with diethyl ether. The products (**1–16**) were further recrystallized in methanol. All synthesized compounds **1–16** were fully characterized by different spectroscopic method. (Scheme 1, Table 1).

2.2. Structure-activity relationship

All the synthesized analogs were screened for their potential acetylcholinesterase and butyrylcholinesterase inhibition activi-

ties. Most of the analogs of the series exhibited good inhibition potential when compared to the standard drug donepezil having an IC_{50} value of 0.016 ± 0.12 for acetylcholinesterase and 0.30 ± 0.010 for butyrylcholinesterase. The most potent analog among the series was analog **2** having three hydroxyl group on the phenyl ring. The IC_{50} values for this analog was 0.10 ± 0.01 for acetylcholinesterase and 0.30 ± 0.01 for butyrylcholinesterase. The high inhibition potential of this analog might be due to the participation of hydroxyl groups in hydrogen bonding with the active sites of enzymes (Hussain et al., 2022).

Similarly, if we compare the analogs **1**, **5**, **10**, **11** and **12** these analogs have two hydroxyl groups on phenyl ring, but their position is different. The most active analog among them is analog **10** having an IC_{50} value of 0.10 ± 0.01 for acetylcholinesterase and 0.20 ± 0.01 for butyrylcholinesterase, this may be due to intramolecular hydrogen bonding of compound **10** which makes it more proton donor. The analog **1** having hydroxyl group at 2 and 3 position has an IC_{50} value of 0.20 ± 0.01 and 0.40 ± 0.01 for acetylcholinesterase and butyrylcholinesterase respectively. The higher activity of compound **1** due to same reason intramolecular hydrogen bonding. The IC_{50} values of analogs **5, 11** and **12** are almost close to each other. The slight difference in their inhibition potential might be due to the difference in the position of hydroxyl group on phenyl ring which may interact with enzymes in different ways.

Similarly, if we compare the analogs **3, 6** and **15**, these analogs have only one hydroxyl group on the phenyl ring, but its position is different. The activity of analog **6** having hydroxyl group at *para* position is superior to **3** and **15** having hydroxyl group at *ortho* and meta positions respectively. The IC_{50} value of this analog is 0.80 ± 0.01 for acetylcholinesterase and 1.30 ± 0.10 for butyrylcholinesterase respectively. The IC_{50} value of analog **3** having hydroxyl group at meta position is 1.80 ± 0.10 for AChE and 2.10 ± 0.10 for BChE and that of analog **15** is 2.70 ± 0.10 and 2.90 ± 0.10 for AChE and BChE respectively.

The interaction between analogs and the ligand protein is not equally favored by identical substituents on the phenyl ring therefore, analogs **4, 7** and **8** have fluoro group on phenyl ring, but their position is different. Analog **4** having fluoro group at *ortho* position has an IC_{50} value of 0.70 ± 0.01, analog **7** having fluoro group at *para* position has an IC_{50} value of 0.30 ± 0.01 and analog **8** having fluoro group at meta position has a value of 0.90 ± 0.01. This shows that fluoro group at *para* position is promising for interactions with the active sites of enzymes (Hussain et al., 2022). The analogs **13** and **14** have methyl groups at position 3 and 4 of phenyl ring. The analog **13** has methyl group at meta position is superior in activity (IC_{50} = 4.80 ± 0.20 for AChE and 5.10 ± 0.10 for BChE) than the analog **14** having methyl group at *para* position (IC_{50} = 8.30 ± 0.30 for AChE and 8.30 ± 0.10 for BChE). Analog **9** having dimethylamino group also exhibited good activity having IC_{50} value of 2.10 ± 0.10 for AChE and 2.60 ± 0.01 for BChE. The analog **16** having methoxy group displayed moderate activity having IC_{50} value of 9.10 ± 0.20 and 8.90 ± 0.20 for AChE and BChE respectively.

2.3. Docking analysis of acetylcholinesterase and butyrylcholinesterase

The molecular docking studies had been performed to visualize plausible binding interactions that can form between active compounds with acetylcholinesterase and butyrylcholinesterase. Prior to performing molecular docking studies, validation had been carried out for both crystal structures, acetylcholinesterase and butyrylcholinesterase using their co-crystallized ligands (Fig. 1). It was observed that validation for butyrylcholinesterase through redocking of the co-crystallized ligand, butyrylthiocholine (BTC), gives a rmsd value of 1.7Å, while redocking of donepezil against acetylcholinesterase recorded lower rmsd value of 0.8Å. These
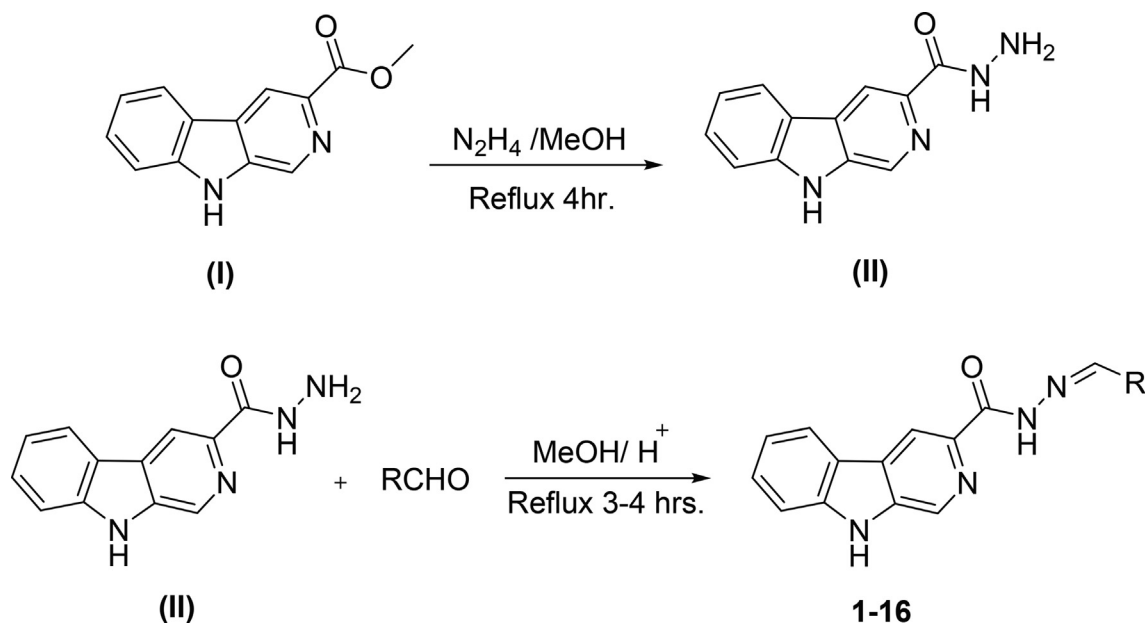
Scheme 1. Synthesis of (*E*)-*N*′-aryl-9*H*-pyrido[3,4-b]indole-3-carbohydrazide (**1–16**).

rmsd values, which are less than 2Å, indicate that the molecular docking protocol is well established for the target proteins.

The molecular docking results for compound **2** against acetylcholinesterase showed that hydroxyl (OH) group at *para* position can possibly form a conventional hydrogen bonding with the backbone (O) of Gly120 (2.03Å) while the other hydroxyl group at *meta* position displayed the ability to form a conventional hydrogen bonding with side chain (OE1) of Glu202 at the distance of 1.96Å (Fig. 2). These interactions were stabilized by hydrophobic π-π stacking interactions between the extended ring and the indole sidechain of Trp86. As for the hydrazone linkage, flexibility allows the methine (=CH) moiety to form a carbon hydrogen bond with the backbone (O) of His447 (2.60Å).
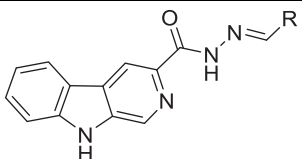
On the *β*-carboline moiety, methine (=CH) group next to the nitrogen of the pyridine ring can form a carbon hydrogen bonding with sidechain (OD2) of Asp74 (2.67Å). The *β*-carboline can be further stabilized via several hydrophobic π-π stacking involving residues Tyr124, Tyr337, Tyr341, and Trp286. Comparison between compound 2 and 10 showed that the extended aromatic ring can be positioned in such a way that allows the hydroxyl group at *meta* position to either act as a hydrogen bond donor to form interaction with Glu202 or a hydrogen bond acceptor to interact with His447. The extended ring of compound 10 was stabilized by a hydrophobic amide-π stacking interaction with residue Gly120. Docking results displayed that compound **1** is extended towards the interior cavity allowing the hydroxyl group (OH) at meta position to act as hydrogen bond donor and form a conventional hydrogen bond interaction with the sidechain phenolic OH of Tyr133 (2.04Å). The hydroxyl group at meta position can also form a carbon-hydrogen bond interaction with the sidechain (HA) of Gly126 (2.51Å). On the other hand, the carbonyl oxygen can potentially act as hydrogen bond acceptor and form a carbon-hydrogen bond interaction with the sidechain (HD2) of His447 (2.67Å) while *β*-carboline moiety stabilizes the structure through hydrophobic π-π stacking with residues Trp286 and Tyr341, and a π-π T-shaped interaction Tyr124.
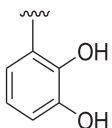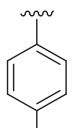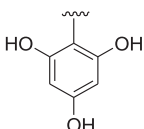
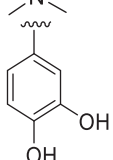Further analysis on molecular docking results for active compounds **5**, **11**, and **12** suggested that presence of hydroxyl group played a crucial role in establishing interaction with active residues Gly120, Tyr133, and Glu202 as being observed for the most active compounds **1**, **2**, and **10** (Fig. 3). It was observed for compound 5 that the hydroxyl group at *ortho* position can act as a hydrogen bond donor to form conventional hydrogen bond with the sidechain (OE1) Glu202 (1.91Å) while the hydroxyl group at *para* formed another hydrogen bond interaction with the backbone (O) of Gly120 at the distance of 2.07 Å. On the other hand, molecular docking result for compound **11** suggests that the hydroxyl group at *para* position can possibly act as a hydrogen bond donor to form hydrogen bond interaction with either the backbone (O) of Gly120 (2.72Å), the backbone (HH) of Tyr133 (2.83 Å), or the sidechain (OE1) of Glu202 (1.89Å). As for compound **12**, the hydroxyl group at meta position was observed to form similar interactions as compound **11**. In this case, the hydroxyl group at meta position can possibly form hydrogen bonding with the backbone (O) of Gly120 (2.50 Å), the backbone (HH) of Tyr133 (2.58 Å), or the sidechain (OE1) of Glu202 (1.89 Å). In both cases, the hydroxyl at *ortho* position for compound **11** and the second hydroxyl group at meta position of compound **12** did not participate in any interaction, indicating that additional hydroxyl group on the extended aromatic group is not very crucial for the activity.
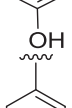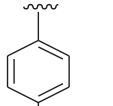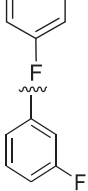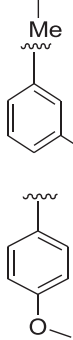
The fact that the inhibition activity displayed by the derivatives does not depend on additional hydroxyl groups attached to the extended ring was further supported by docking results for compounds **3**, **6**, and **15** which clearly showed that the hydroxyl groups at various positions can possibly interact with either Gly202 or Tyr133 inhibit acetylcholinesterase (Fig. 4). The docking result for compound **3** suggests that hydroxyl at *ortho* position can form a hydrogen bonding interaction with the side chain (OE1) of Glu202 (1.89 Å). Similarly observed for compound **6**, the hydroxyl group at *para* position can also form a hydrogen bonding with side chain (OE1) Glu202 at the distance of 1.96 Å. For compound 3, the hydroxyl group at meta position formed a hydrogen bonding with the backbone (HH) of active residue Tyr133 (3.02 Å). The results showed similar pattern for derivatives with mono-fluoro substituent on the extended aromatic. Compounds **4**, and **7** displayed better activity as compared to disubstituted compounds. Molecular docking results for compound **4** suggest that the fluorine at meta position can possibly form a halide bond with the sidechain (HA2) of Gly121 (2.72 Å). On the other hand, docking results also showed that fluorine substituent of compounds **7** can form a halide bond interaction with Glu202 through its sidechain (HE2) at the distance of 2.37 Å.

Table 1
Acetylcholinesterase and butyrylcholinesterase inhibition activity of β-carboline hydrazide.

S. No	R	AChE IC$_{50}$ (μM ± SEM)	BuChE IC$_{50}$ (μM ± SEM)	S. No	R	AChE IC$_{50}$ (μM ± SEM)	BuChE IC$_{50}$ (μM ± SEM)
1		0.20 ± 0.01	0.40 ± 0.01	9		2.10 ± 0.10	2.60 ± 0.10
2		0.10 ± 0.01	0.30 ± 0.01	10		0.10 ± 0.01	0.20 ± 0.01
3		1.80 ± 0.10	2.10 ± 0.10	11		1.10 ± 0.10	1.30 ± 0.10
4		0.70 ± 0.01	0.40 ± 0.10	12		1.30 ± 0.10	1.60 ± 0.10
5		1.30 ± 0.10	1.10 ± 0.10	13		4.80 ± 0.20	5.10 ± 0.10
6		0.80 ± 0.01	1.30 ± 0.10	14		8.30 ± 0.30	8.30 ± 0.10
7		0.30 ± 0.01	0.60 ± 0.01	15		2.70 ± 0.10	2.90 ± 0.10
8		0.90 ± 0.01	1.30 ± 0.10	16		9.10 ± 0.20	8.90 ± 0.20
Standard				Donepezil		0.016 ± 0.12	0.30 ± 0.010
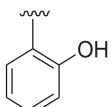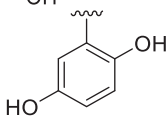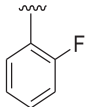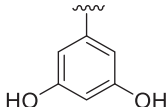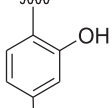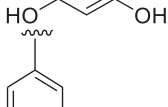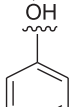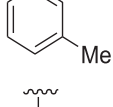
For inhibition of butyrylcholinesterase, compound **10** hydroxyl groups at *ortho* and *para* position can possibly form conventional hydrogen bonding interactions with backbone (OE1) of residue Glu197 at the distance of 1.99Å and 1.97Å (Fig. 5). The hydroxyl group at *para* position can also form a hydrogen bonding with backbone (NH) of Gly115 (2.35Å) and the sidechain (HH) of residue Tyr128 (2.31Å). The extended ring can be further stabilized via amide π-stacking involving the backbone of Gly115. Besides that, observation also showed that methine (CH) moiety can also form a carbon hydrogen bond with the sidechain (OG1) of residue Thr120 (3.05Å). β-carboline moiety on the other hand forms an electrostatic π-anion interaction with the sidechain (OD2) of residue Asp70 and multiple π-π stacking interactions with residue Tyr332 via its π-orbital. As for compound 2, hydroxyl at *para* posi-

tion of the extended ring can either act as a hydrogen bond donor to interact with sidechain (OE1) of residue Glu197 (1.91Å) or a hydrogen bond donor to interact with sidechain hydroxyl group (OH) of residue Tyr128 (1.89Å). On the other hand, it was observed that the other hydroxyl group at *ortho* position can form another hydrogen bond with the sidechain (OG1) of residue Thr120 (2.80Å). The compound is positioned in a way that allows the oxygen of the carbonyl (C = O) group to form a hydrogen bonding with sidechain (HG1) of residue Thr120 (2.13Å). The imine nitrogen can act as a hydrogen bond acceptor for carbon-hydrogen bond interaction with the sidechain (HA2) of residue Gly116 (2.67Å). The β-carboline moiety is stabilized via a hydrophobic π-alkyl interaction with Ala277. The molecular docking results for compound **1** showed that the extended ring flipped in such a way that both
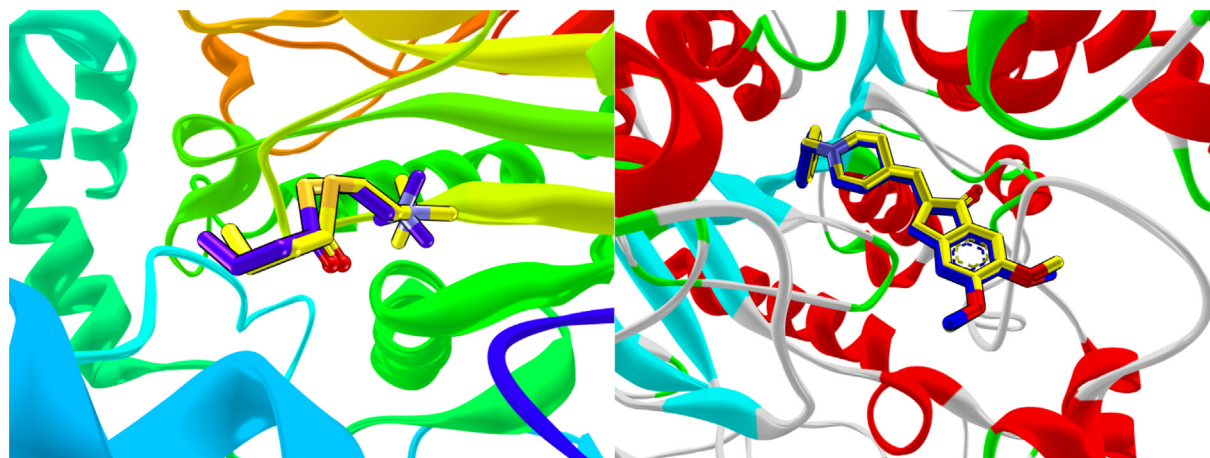
Fig. 1. **(a)** Redocked butyrylthiocholine overlapping with co-crystallized butyrylthiocholine in the active site of BChE with rmsd of 1.7Å; **(b)** Redocked donepezil aligned well with co-crystallized donepezil in the active site of AChE with rmsd of 0.8Å.

hydroxyl groups can act as hydrogen bond donor to form hydrogen bond interactions with the sidechain (OE1) of active site residue Glu197 at the distance of 1.97Å and 2.07A. The extended ring was further stabilized via several hydrophobic interactions that includes a π-π T-shaped interaction with the residue His438 and two π-π T-shaped interactions with residue Trp82. The ring was also stabilized by an additional electrostatic π-cation interaction with the sidechain (NE2) of residue His438. The hydroxyl group at *ortho* position extended towards residue Ser198 to form a carbon hydrogen interaction with its sidechain (HB1) at the distance of 2.51Å. Another carbon hydrogen bond was observed between methine (=CH) and Ser198 which took place through the side chain (H35) at the distance of 2.72Å. The carbonyl oxygen on hydrazone linkage can act as a hydrogen bond donor to form another carbon hydrogen interaction with the sidechain (HA) of Leu286 (2.77Å).

2.4. Molecular dynamics

Molecular dynamics simulation was performed for both AChE and BChE. Analysis on molecular dynamics trajectory of compound **2**-AChE complex showed that the protein–ligand is stable (Fig. 6a). The RMSD values for acetylcholinesterase suggested that there are no large conformational changes in the protein structure as indicated by maximum rmsd value of 0.29A. As for compound **2**, there were no large conformational changes for the first 40 ns. A significant conformational change was observed after 40 ns which then remained stable towards the end of the simulation. The RMSF of compound **2** showed that β-carboline moiety fluctuated the most compared to the rest of the compound with carbons C_{11}, C_{12}, and C_{13} displaying among highest RMSF value (Fig. 6b). It was also observed that the oxygen atoms O25, O26, and O27 displayed low RMSF values which allows conformational changes in the binding position affecting crucial interactions. Similar observation was observed for compound **10** in complex with BChE. It was observed that the protein is quite stable with no major fluctuation in rmsd values throughout the simulation (Fig. 6c). Compound **10** displayed slight rmsd value fluctuation throughout the simulation. Both proteins and ligands displayed maximum rmsd values of not more than 3A indicating formation of stable complexes. Unlike compound **2**, the β-carboline moiety for compound **10** in complex with BChE displayed low RMSF values with most fluctuation coming from the extended aromatic moiety (Fig. 6d). The RMSF plot also showed that the oxygen atom O_{26} fluctuated more than O_{25}. This clearly indicates that oxygen atom O_{25} can form more stable hydrogen bonding compared to O_{26}.

In the torsional plot of compound **2** it was observed that the bond between carbonyl and β-carboline moiety was quite rigid with a maximum rotatability of up to 45° angle throughout the simulation (Fig. 7a). Some of the most flexible bonds for compound **2** that were to rotate up to 180° angle throughout the simulation includes the bonds between *para/ortho* hydroxyl groups and benzene ring. On the other hand, the bond between the nitrogen atoms of the hydrazone linkage was less flexible compared to the hydroxyl bonds with larger rotatability range between 45°-180° angle. Comparison between compound **2** and **10** showed not much difference except for the bond between the nitrogen atoms of the hydrazone linkage for compound **10** which displayed higher rotatability (Fig. 7b). This could be due to lack of hydroxyl group at *ortho* position on compound **10** which lead to lack of intramolecular hydrogen bonding with nitrogen of hydrazone linkage as observed in compound **2**.

3. Conclusions

In conclusion, we have synthesized sixteen analogs of β-carboline hydrazides due to biological importance of both carboline nucleus and hydrazides. The newly synthesized analogs were evaluated using spectroscopic methods like 1H NMR and 13C NMR. The synthesized analogs were screened for the inhibition of acetylcholinesterase and butyrylcholinesterase enzymes. Comparing the inhibition potential of all the synthesized analogs with reference drug shows that most of the analogs displayed good inhibition potential. Moreover, according to the structure–activity relationship, the number, type and position of substituents also played a key role in inhibition which make more interactive or less interactive with enzymes. The most potent inhibitors of the AChE and BChE were those having hydroxyl groups on phenyl ring due to the participation of these substituents in H-bonding with the active site of the enzyme. Additionally, molecular docking research was carried out to investigate the interactions of the synthesized compounds with the active sites of enzymes and the results verified the experimental results.

4. Experimental

4.1. General procedure for the synthesis of the compounds

The Methyl 9H-pyrido[3,4-b]indole-3-carboxylate (5 g, 22.12 mmol) (**I**) was refluxed with mixture of hydrazine hydrate (25 mL) and methanol (25 mL) to form 9H-pyrido[3,4-b]indole-3-carbohydrazide (4.5 g, 19.9 mmol) (**II**) 4 h. The 9H-pyrido[3,4-b]i
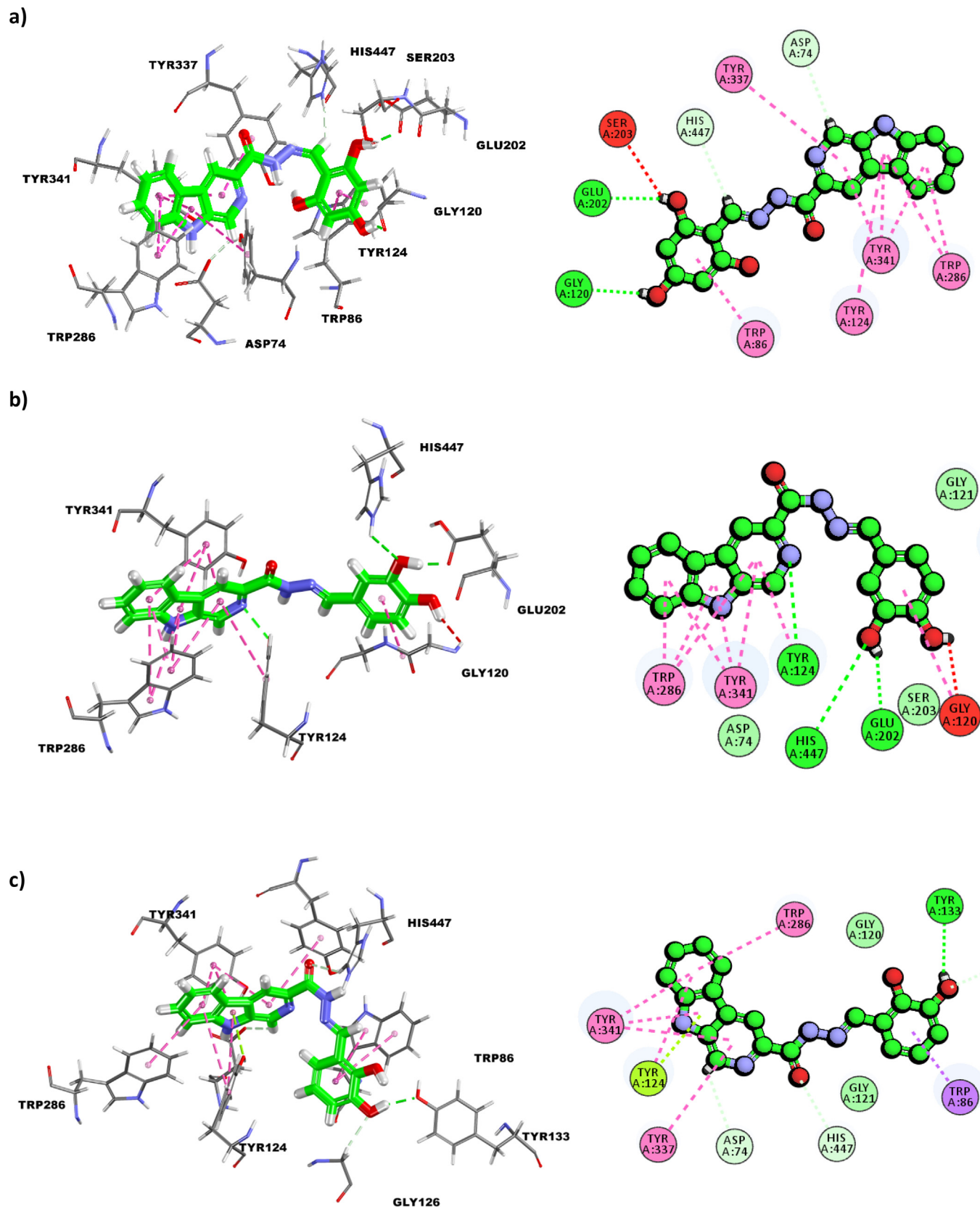
Fig. 2. (a) Binding interactions and 2D-interaction diagram of compound **2** with acetylcholinesterase; (**b**) Binding interactions and 2D-interaction diagram of compound **10** with acetylcholinesterase; (**c**) binding interactions and 2D-interaction diagram of compound **1** with acetylcholinesterase.
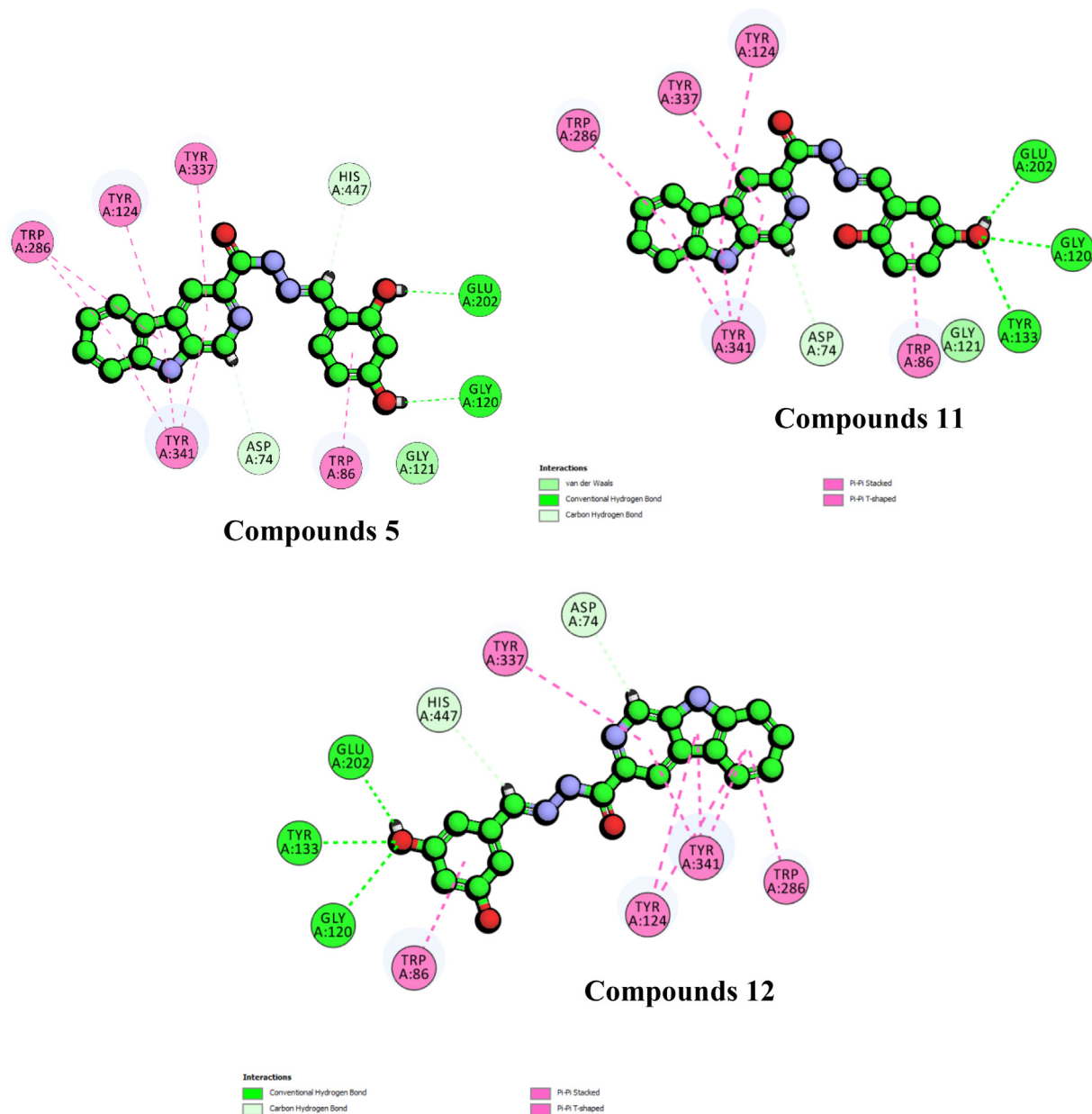
Fig. 3. (a) 2D-interaction diagram for compound **5**, **11**, and **12** against acetylcholinesterase.

ndole-3-carbohydrazide (**II**) (0.226 g, 1 mmol) was treated with various aryl aldehyde (1 mmol) in methanol (15 mL) along with catalytic amount of acetic acid for 3–4 h to obtained (*E*)-*N'*-aryl-9 H-pyrido[3,4-b]indole-3-carbohydrazide (**1–16**). The completion of reaction was monitored by TLC and after completion of reaction the solvent was evaporated and obtained crude product was washed with diethyl ether. The products (**1–16**) were further recrystallized in methanol. All synthesized compounds **1–16** were fully characterized by different spectroscopic methods.

4.2. Characterization data for compounds

4.2.1. (E)-N'-(2,3-dihydroxybenzylidene)-9H-pyrido[3,4-b]indole-3-carbohydrazide (1)

^{1}H NMR (500 MHz, DMSO d_6): δ 12.52 (s, 2H, 2xNH,), 12.09 (s, 1H, OH), 11.64 (s, 1H, OH), 9.10 (s, 1H, H-C = N), 8.96 (s, 1H, pyrido-H), 8.85 (s, 1H, pyrido-H), 8.46 (d, *J* = 7.8, 1H, Ar), 7.75 (d, *J* = 8.0 Hz, 1H, Ar), 7.68 (t, *J* = 7.5 Hz, 1H, Ar), 7.37 (t, *J* = 7.5 Hz,

1H, Ar), 6.92–6.87 (m, 2H, Ar), 6.77 (dd, *J* = 6.0, 2.0 Hz, 1H, Ar); IR (KBr): 3425 cm^{-1} (OH-str), 3264 cm^{-1} (2° amine N–H Str), 1606 cm^{-1} (Ar C = C), 1551 cm^{-1} (N–H Bend), 1233 cm^{-1} (C-N str); ^{13}C NMR (125 MHz, DMSO d_6): δ 161.72, 150.22, 146.65, 146.09, 141.53, 138.91, 137.94, 132.95, 129.29, 128.74, 122.86, 121.39, 120.93, 120.69, 119.58, 119.21, 117.79, 115.74, 112.83; HREI-MS: *m/z* calcld for $C_{19}H_{14}N_4O_3$, [M]$^+$ 346.1066 Found 346.1047.

4.2.2. (E)-N'-(2,4,6-trihydroxybenzylidene)-9H-pyrido[3,4-b]indole-3-carbohydrazide (2)

^{1}H NMR (500 MHz, DMSO d_6): δ 12.32 (s, 1H, NH), 12.03 (s, 1H, NH), 11.20 (s, 1H, OH), 9.81 (s, 1H, OH), 8.97 (s, 1H, OH), 8.95 (s, 1H, H-C = N), 8.94 (s, 1H, pyrido-H), 8.82 (s, 1H, pyrido-H), 8.43 (d, *J* = 7.7, 1H, Ar), 7.68 (d, *J* = 7.8 Hz, 1H, Ar), 7.62 (t, *J* = 7.5 Hz, 1H, Ar), 7.32 (t, *J* = 7.4 Hz, 1H, Ar), 5.84 (s, 2H, Ar); IR (KBr): 3375 cm^{-1} (OH-str), 3322 cm^{-1} (2°amine N–H Str), 1640 cm^{-1} (C = O), 1611 cm^{-1} (Ar C = C), 1584 cm^{-1} (N–H Bend),
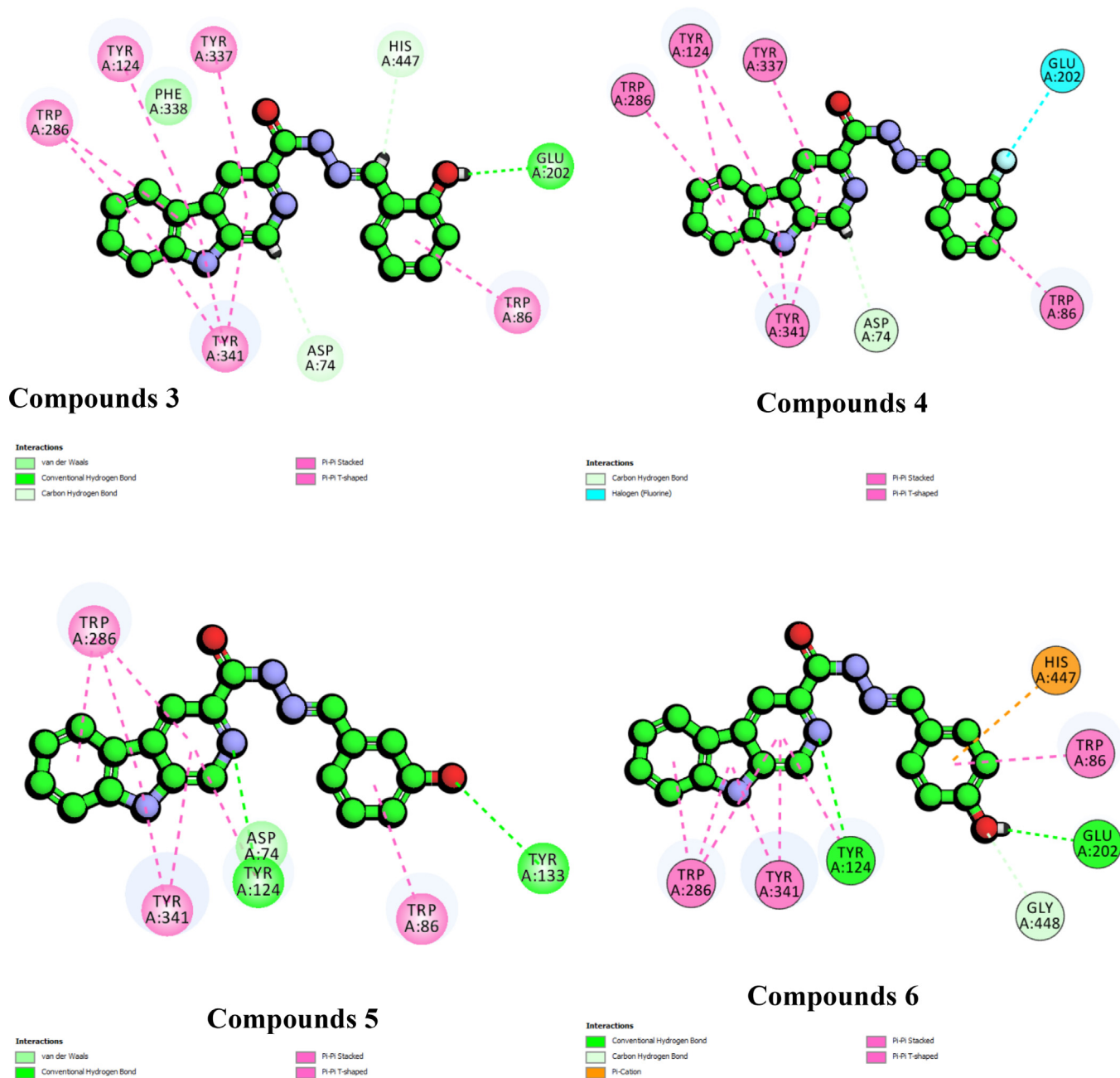
Fig. 4. The 2D-interaction diagram for compounds **3**, **4**, **5**, **6**, and **7** against acetylcholinesterase.

1251 cm^{-1} (C-N str), 1162 cm^{-1} (C-O str); ^{13}C NMR (125 MHz, DMSO d_6): δ 164.55, 161.78, 161.28, 160.21, 147.58, 141.50, 139.30, 137.80, 132.87, 128.69, 122.80, 121.39, 120.61, 115.38, 112.80, 110.04, 99.90, 94.80, 92.49; HREI-MS: *m/z* calcld for C$_{19}$H$_{14}$N$_4$O$_4$, [M]$^+$ 362.1015 Found 362.1003.

str), 1121 cm^{-1} (C-O str); ^{13}C NMR (125 MHz, DMSO d_6): δ 163.26, 161.74, 159.12, 158.10, 149.64, 141.54, 138.93, 137.94, 133.69, 132.94, 120.68, 120.06, 119.78, 119.16, 118.66, 117.00, 116.95, 115.71, 112.83; HREI-MS: *m/z* calcld for C$_{19}$H$_{14}$N$_4$O$_2$, [M]$^+$ 330.1117 Found 330.1104.

4.2.3. (E)-N'-(2-hydroxybenzylidene)-9H-pyrido[3,4-b]indole-3-carbohydrazide (3)

^{1}H NMR (500 MHz, DMSO d_6): δ 12.46 (s, 1H, NH), 12.05 (s, 1H, NH), 11.63 (s, 1H, OH), 9.03 (s, 1H, H-C = N), 8.96 (s, 1H, pyrido-H), 8.86 (s, 1H, pyrido-H), 8.43 (d, *J* = 7.1 Hz, 1H, Ar), 7.72 (d, *J* = 7.5 Hz, 1H, Ar), 7.62 (t, *J* = 6.9 Hz, 1H, Ar), 7.45 (d, *J* = 7.0 Hz, 1H, Ar), 7.40–7.37 (m, 2H, Ar), 6.97–6.90 (m, 2H, Ar-H); IR (KBr): 3338 cm^{-1} (OH-str), 3267 cm^{-1} (2° amine N–H Str), 3040 cm^{-1} (Ar C–H str), 1614 cm^{-1} (Ar C = C), 1562 cm^{-1}(N–H Bend), 1270 cm^{-1} (C-N

4.2.4. (E)-N'-(2-fluorobenzylidene)-9H-pyrido[3,4-b]indole-3-carbohydrazide (4)

^{1}H NMR (500 MHz, DMSO d_6): δ 12.35 (s, 1H, NH), 12.03 (s, 1H, NH), 9.02 (s, 1H, H-C = N), 8.96 (s, 1H, pyrido-H), 8.92 (s, 1H, pyrido-H), 8.44 (d, *J* = 7.4 Hz, 1H, Ar), 8.00 (t, *J* = 7.4 Hz, 1H, Ar), 7.72 (d, *J* = 7.5 Hz, 1H, Ar), 7.61 (t, *J* = 7.4 Hz, 1H, Ar), 7.50 (dd, *J* = 6.5, 2.0 Hz, 1H, Ar), 7.37–7.30 (m, 3H, Ar); IR υ (KBr disk): 3308 cm^{-1} (NH stretch), 3084 cm^{-1} (Ar.C–H stretch), 1633 cm^{-1} (C = O), 1551 cm^{-1} (C = N), 1492 cm^{-1} (C-N), 1311 cm^{-1} (C = C),
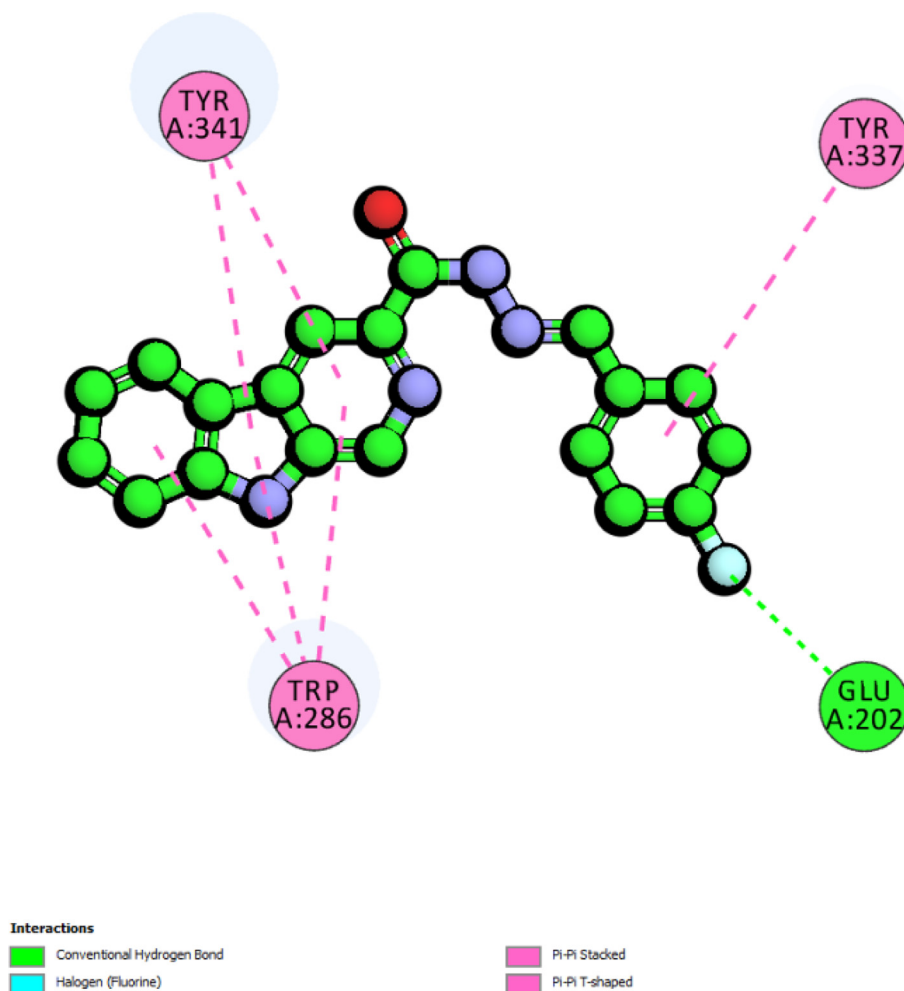
Interactions

■ (green)	Conventional Hydrogen Bond	■ (pink)	Pi-Pi Stacked
■ (cyan)	Halogen (Fluorine)	■ (pink)	Pi-Pi T-shaped

Fig. 4 (*continued*)

1154 cm^{-1} (C-F); ^{13}C NMR (125 MHz, DMSO d_6): δ 162.24, 161.93, 160.25, 141.54, 141.23, 139.28, 137.91, 132.83, 132.23, 129.26, 128.77, 126.94, 125.37, 122.87, 121.40, 120.65, 116.54, 116.37, 112.81; HREI-MS: *m/z* calcld for C$_{19}$H$_{13}$FN$_4$O, [M]$^+$ 332.1073 Found 332.1054.

4.2.5. (E)-N'-(2,4-dihydroxybenzylidene)-9H-pyrido[3,4-b]indole-3-carbohydrazide (5)

^{1}H NMR (500 MHz, DMSO d_6): δ 12.33 (s, 1H, NH), 12.08 (s, 1H, NH), 10.76 (s, 1H, OH), 9.01 (s, 1H, OH), 8.97 (s, 1H, H-C = N), 8.95 (s, 1H, pyrido-H), 8.75 (s, 1H, pyrido-H), 8.45 (d, *J* = 7.5 Hz, 1H, Ar), 7.69 (d, *J* = 7.4 Hz, 1H, Ar), 7.62 (t, *J* = 7.4 Hz, 1H, Ar), 7.36 (t, *J* = 7.5 Hz, 1H, Ar), 6.95 (t, *J* = 7.4 Hz, 1H, Ar), 6.81–6.76 (m, 2H, Ar); IR (KBr): 3411 cm^{-1} (OH-str), 3264 cm^{-1} (2° amine N–H Str), 1633 cm^{-1} (C = O), 1604 cm^{-1} (Ar C = C), 1558 cm^{-1} (N–H Bend), 1237 cm^{-1} (C-N str), 1079 cm^{-1} (C-O str); ^{13}C NMR (125 MHz, DMSO d_6): δ 191.82, 161.63, 150.86, 150.48, 150.30, 149.21, 141.53, 139.04, 137.91, 132.91, 129.28, 128.74, 125.00, 122.84, 120.67, 119.34, 118.73, 115.63, 112.83; HREI-MS: *m/z* calcld for C$_{19}$H$_{14}$N$_4$O$_3$, [M]$^+$ 346.1066 Found 346.1043.

4.2.6. (E)-N'-(4-hydroxybenzylidene)-9H-pyrido[3,4-b]indole-3-carbohydrazide (6)

^{1}H NMR (500 MHz, DMSO d_6): δ 12.03 (s, 1H, NH), 11.87 (s, 1H, NH), 9.76 (s, 1H, OH), 9.00 (s, 1H, H-C = N), 8.95 (s, 1H, pyrido-H), 8.93 (s, 1H, pyrido-H), 7.75 (d, *J* = 7.0 Hz, 1H, Ar), 7.71 (dd, *J* = 7.4, 2.0 Hz, 1H, Ar), 7.66–7.60 (m, 3H, Ar), 7.32 (t, *J* = 7.5 Hz, 1H, Ar),

6.89–6.85 (m, 2H, Ar); IR (KBr): 3351 cm^{-1} (OH-str), 3263 cm^{-1} (2° amine N–H Str), 1631 cm^{-1} (C = O), 1588 cm^{-1} (Ar C = C), 1283 cm^{-1} (C-N str), 1033 cm^{-1} (C-O str); ^{13}C NMR (125 MHz, DMSO d_6): δ 191.38, 163.92, 161.39, 159.81, 148.82, 141.53, 139.56, 137.79, 132.77, 132.56, 129.31, 129.21, 128.77, 126.04, 122.83, 121.40, 120.59, 116.34, 112.78, 56.5093; HREI-MS: *m/z* calcld for C$_{19}$H$_{14}$N$_4$O$_2$, [M]$^+$ 330.1117 Found 330.1101.

4.2.7. (E)-N'-(4-fluorobenzylidene)-9H-pyrido[3,4-b]indole-3-carbohydrazide (7)

^{1}H NMR (500 MHz, DMSO d_6): δ 12.08 (s, 1H, NH), 12.03 (s, 1H, NH), 8.97 (s, 1H, H-C = N), 8.94 (s, 1H, pyrido-H), 8.65 (s, 1H, pyrido-H), 8.43 (d, *J* = 7.8 Hz, 1H, Ar), 7.80 (t, *J* = 8.6 Hz, 1H, Ar), 7.80 (t, *J* = 7.2 Hz, 1H, Ar), 7.68 (t, *J* = 7.5 Hz, 1H, Ar), 7.62 (t, *J* = 7.5 Hz, 1H, Ar), 7.58 (t, *J* = 7.2 Hz, 1H, Ar), 7.36–7.24 (m, 2H, Ar); IR υ (KBr disk): 3302 cm^{-1} (NH stretch), 3080 cm^{-1} (Ar.C–H stretch), 1630 cm^{-1} (C = O), 1550 cm^{-1} (C = N), 1490 cm^{-1} (C-N), 1308 cm^{-1} (C = C), 1210 cm^{-1} (C-F); ^{13}C NMR (150 MHz, DMSO d_6): δ 164.50, 162.53, 161.70, 147.36, 141.54, 139.33, 137.87, 132.81, 131.70, 131.68, 129.70, 129.64, 129.25, 128.78, 121.40, 120.64, 116.29, 115.51, 112.80; HREI-MS: *m/z* calcld for C$_{19}$H$_{13}$FN$_4$O, [M]$^+$ 332.1073 Found 332.1052.

4.2.8. (E)-N'-(3-fluorobenzylidene)-9H-pyrido[3,4-b]indole-3-carbohydrazide (8)

^{1}H NMR (500 MHz, DMSO d_6): δ 12.18 (s, 1H, NH), 12.02 (s, 1H, NH), 8.97 (s, 1H, H-C = N), 8.95 (s, 1H, pyrido-H), 8.65 (s, 1H,
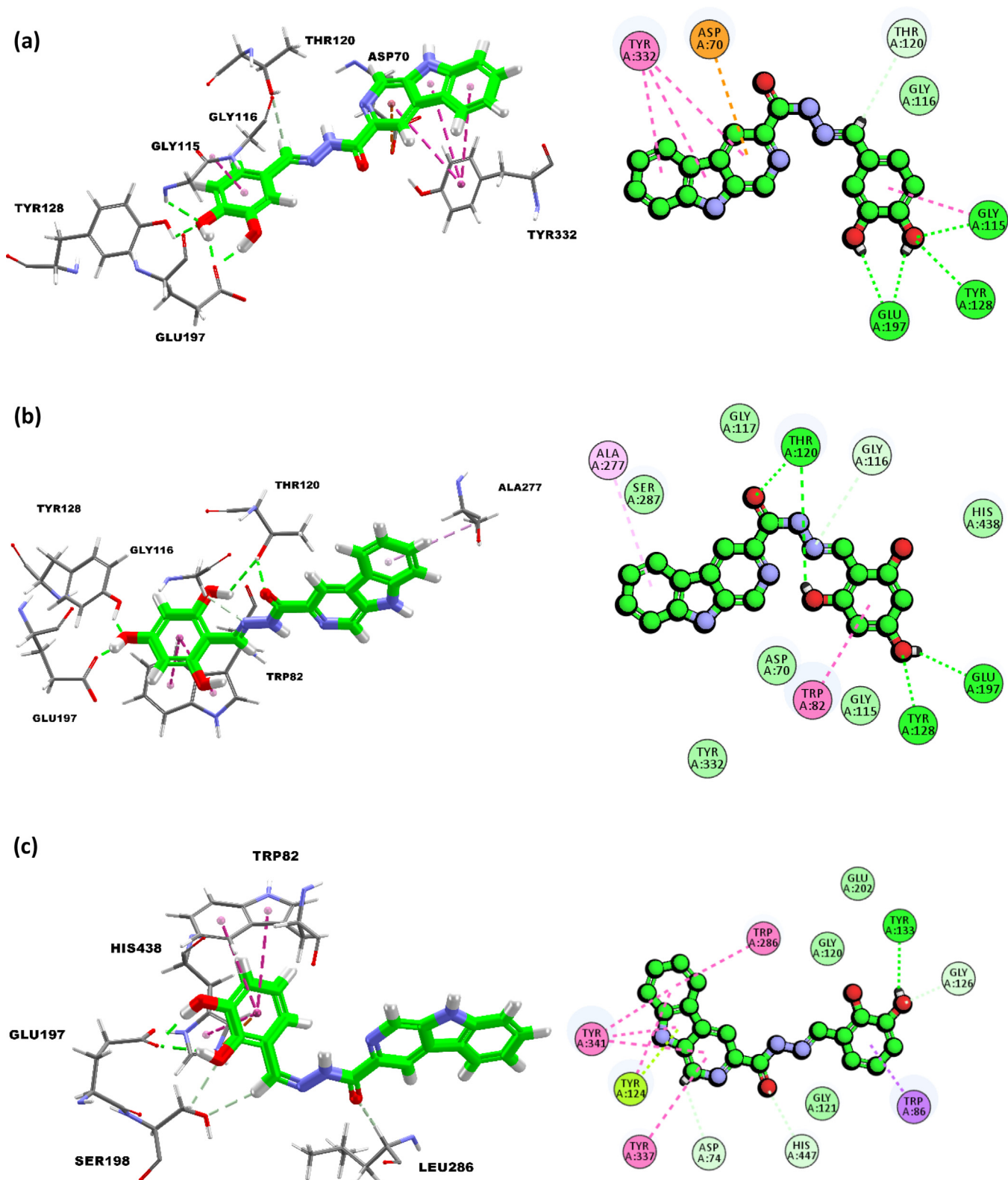
Fig. 5. **(a)** Binding interactions and 2D-interaction diagram of compound **10** with butyrylcholinesterase; b) Binding interactions and 2D-interaction diagram of compound **2** with butyrylcholinesterase; **(c)** binding interactions and 2D-interaction diagram of compound **1** with butyrylcholinesterase.

pyrido-H), 8.44 (d, *J* = 7.6 Hz, 1H, Ar), 7.68 (d, *J* = 7.5 Hz, 1H, Ar), 7.62 (t, *J* = 7.4 Hz, 1H, Ar), 7.60–7.54 (m, 3H, Ar), 7.33–7.25 (m, 2H, Ar); IR υ (KBr disk): 3301 cm^{-1} (NH stretch), 3087 cm^{-1} (Ar.

C–H stretch), 1631 cm^{-1} (C = O), 1554 cm^{-1} (C = N), 1496 cm^{-1} (C-N), 1307 cm^{-1} (C = C), 1230 cm^{-1} (C-F); ^{13}C NMR (125 MHz, DMSO d_6): δ 163.89, 161.82, 147.12, 141.54, 139.23, 137.90,

(a)

(b)

Fig. 6. (a) The RMSD value for compound **2** in complexed with acetylcholinesterase; (**b**) RMSF value for compound **2**; (**c**) RMSD value for compound **10** in complexed with butyrylcholinesterase; (**d**) RMSF value for compound **10**.

(c)

(d)

Fig. 6 (*continued*)

137.72, 132.84, 131.47, 131.39, 129.28, 128.78, 124.00, 122.89, 121.40, 120.67, 115.62, 113.38, 112.81; HREI-MS: *m/z* calcld for $C_{19}H_{13}FN_4O$, [M]$^+$ 332.1073 Found 332.1058.

4.2.9. (E)-N'-(4-(dimethylamino)benzylidene)-9H-pyrido[3,4-b]indole-3-carbohydrazide (9)

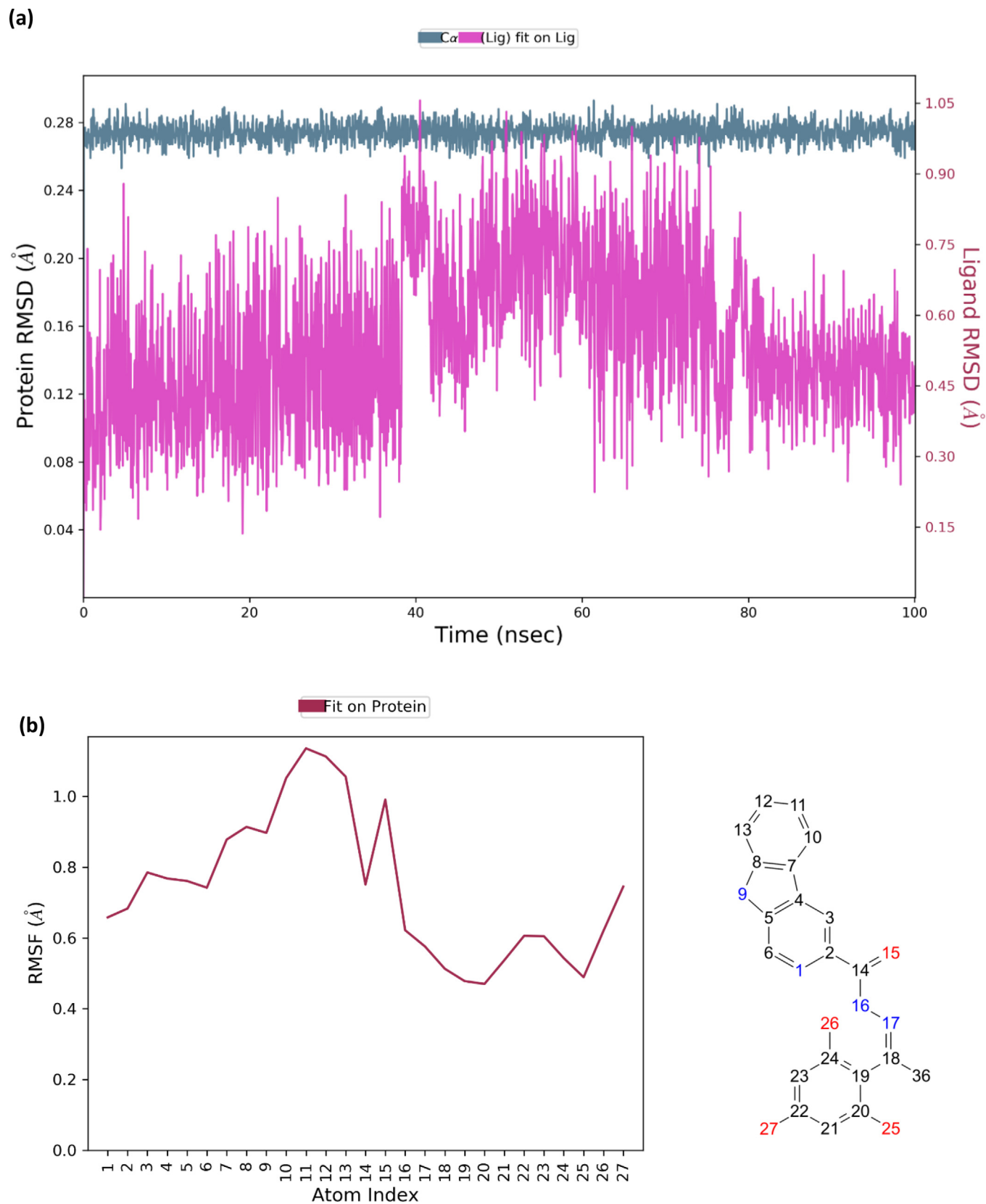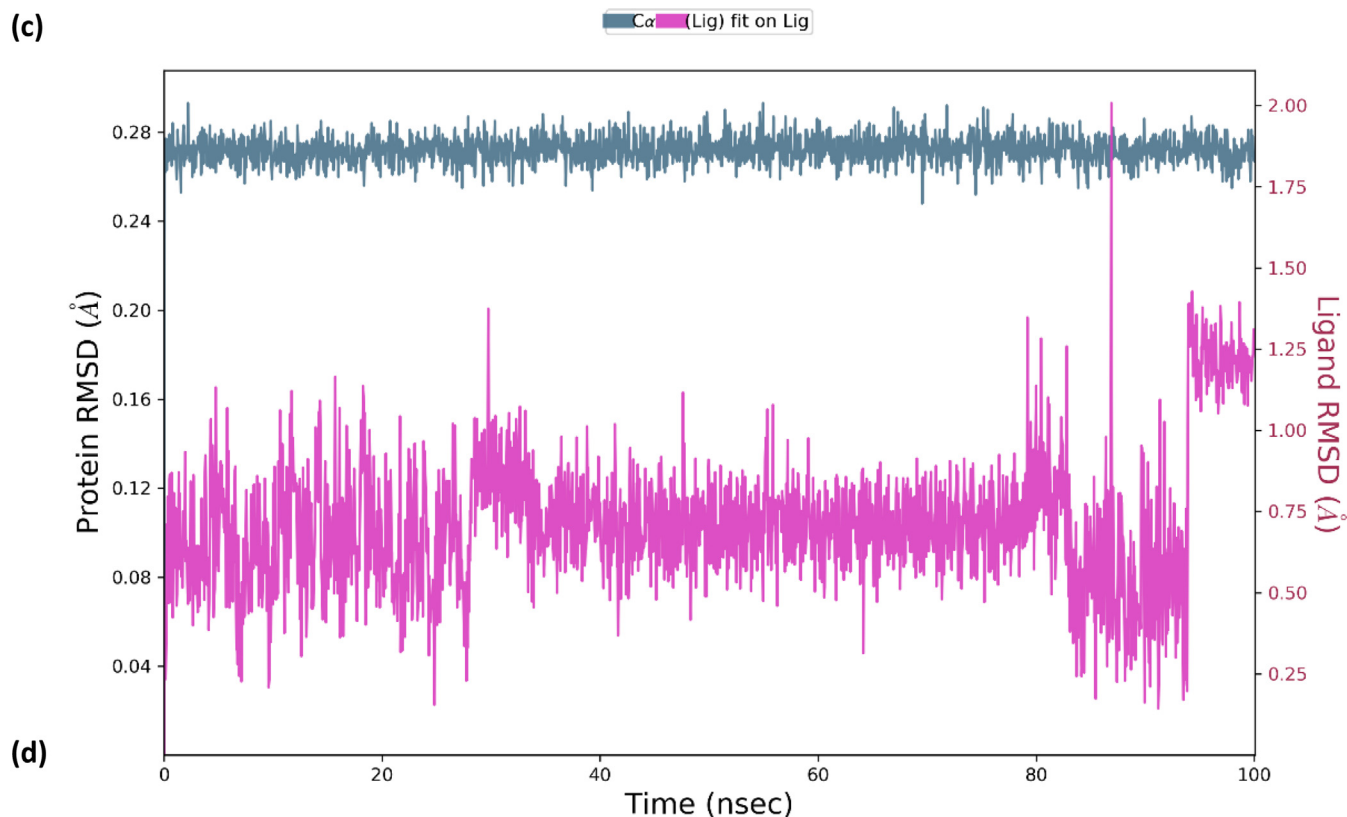^{1}H NMR (500 MHz, DMSO d_6): δ 12.04 (s, 1H, NH), 11.79 (s, 1H, NH), 8.97 (s, 1H, H-C = N), 8.96 (s, 1H, pyrido-H), 8.53 (s, 1H, pyrido-H), 8.48 (d, J = 7.5 Hz, 1H, Ar), 7.67 (dd, J = 7.0, Hz, 1H, Ar), 7.62 (t, J = 7.4 Hz, 1H, Ar), 7.58 (d, J = 7.8 Hz, 2H, Ar), 7.32 (t, J = 7.4 Hz, 1H, Ar), 6.78 (d, J = 7.8 Hz, 2H, Ar), 2.96 (s, 6H, N(CH$_3$)$_3$); IR υ (KBr disk): 3472 cm^{-1} (C-N-C), 3283 cm^{-1} (NH stretch), 3040 cm^{-1} (Ar.C–H stretch), 1637 cm^{-1} (C = O),

1558 cm^{-1} (C = N), 1477 cm^{-1} (C-N); ^{13}C NMR (125 MHz, DMSO d_6): δ 199.94, 151.94, 149.27, 148.80, 146.76, 142.56, 141.52, 139.70, 137.65, 135.73, 132.75, 128.92, 122.84, 122.34, 121.40, 120.59, 115.15, 112.77, 112.29, 35.60, 34.95; HREI-MS: *m/z* calcld for $C_{21}H_{19}N_5O$, [M]$^+$ 357.1590 Found 357.1509.

4.2.10. (E)-N'-(3,4-dihydroxybenzylidene)-9H-pyrido[3,4-b]indole-3-carbohydrazide (10)

^{1}H NMR (500 MHz, DMSO d_6): δ 11.82 (s, 2H, 2xNH), 10.70 (s, 1H, OH), 9.35 (s, 1H, OH), 8.97 (s, 1H, H-C = N), 8.92 (s, 1H, pyrido-H), 8.44 (s, 1H, pyrido-H), 8.41 (d, J = 7.5, Hz, 1H, Ar), 7.67 (d, J = 7.5, Hz, 1H, Ar), 7.62 (t, J = 7.5 Hz, 1H, Ar), 7.32 (t, J = 7.6 Hz, 1H, Ar), 7.26 (t, J = 7.4 Hz, 1H, Ar), 6.93 (dd, J = 7.2,
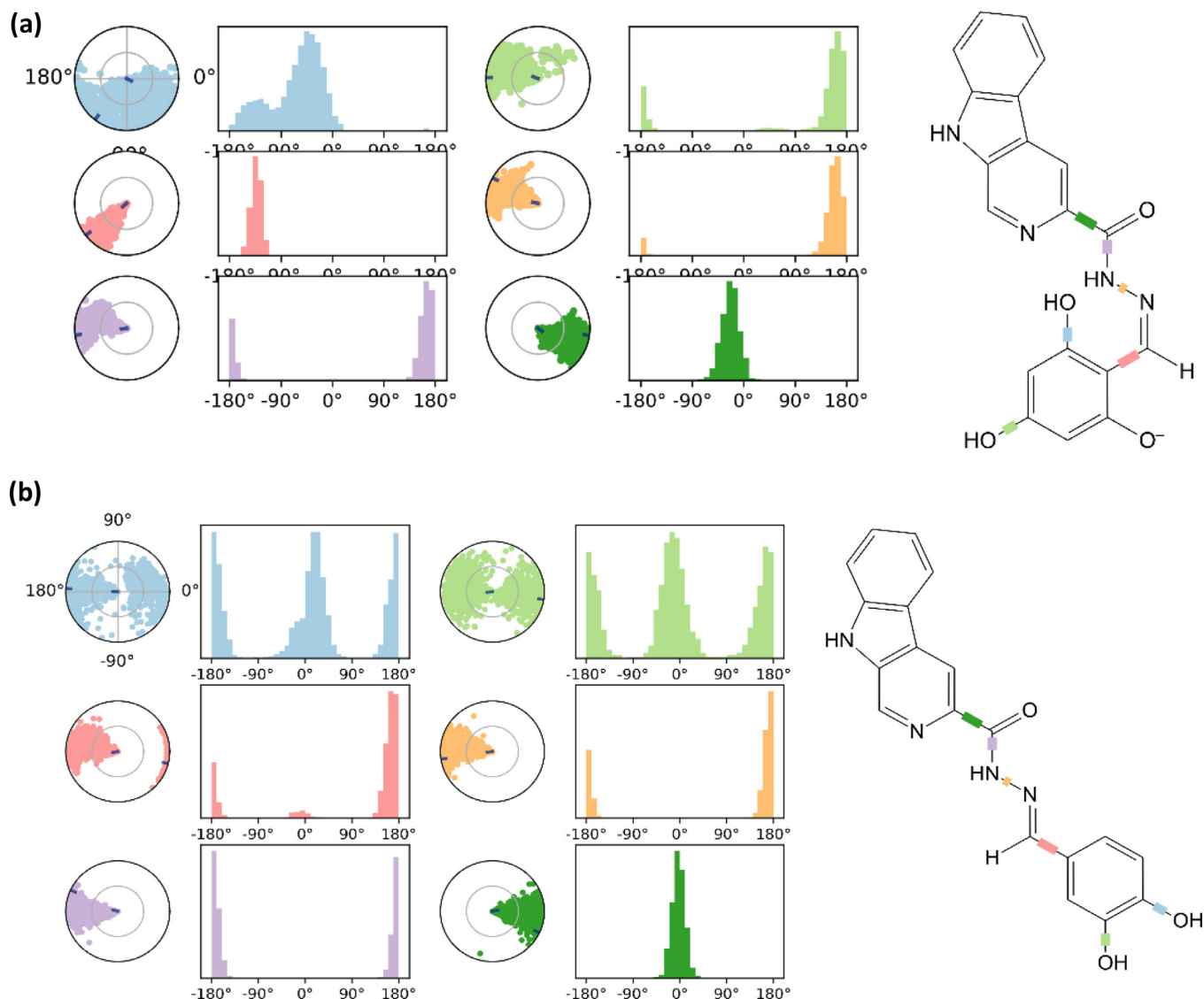
Fig. 7. (a) Torsions plot on conformational evolution of every rotatable bond for compound **2**; (b) Torsions plot on conformational evolution of every rotatable bond for compound **10**.

2.0 Hz, 1H, Ar), 6.80 (d, J = 7.0 Hz, 1H, Ar); IR (KBr): 3414 cm^{-1} (OH-str), 3240 cm^{-1} (2° amine N–H Str), 3028 cm^{-1} (Ar CH str), 1621 cm^{-1} (C = O), 1552 cm^{-1} (N–H Bend), 1254 cm^{-1} (C-N str), 1140 cm^{-1} (C-O str); ^{13}C NMR (125 MHz, DMSO d_6): δ 161.31, 148.99, 148.32, 146.18, 141.53, 139.62, 137.77, 132.75, 129.23, 128.78, 126.52, 122.84, 121.41, 120.92, 120.60, 116.07, 115.26, 113.31, 112.78; HREI-MS: m/z calcld for C$_{19}$H$_{14}$N$_4$O$_3$, [M]$^+$ 346.1066 Found 346.1051.

4.2.11. (E)-N'-(2,5-dihydroxybenzylidene)-9H-pyrido[3,4-b]indole-3-carbohydrazide (11)
^{1}H NMR (500 MHz, DMSO d_6): δ 12.18 (s, 1H, NH), 12.05 (s, 1H, NH), 10.80 (s, 2H, 2xOH), 9.03 (s, 1H, H-C = N), 8.95 (s, 1H, pyrido-H), 8.72 (d, J = 6.5 Hz, 1H, Ar), 8.43 (s, 1H, pyrido-H), 7.72 (d, J = 6.8 Hz, 1H, Ar), 7.60 (d, J = 7.6 Hz, 1H, Ar), 7.32 (d, J = 7.0 Hz, 1H, Ar), 7.23 (d, J = 7.6 Hz, 1H, Ar), 6.40 (dd, J = 7.5, 20 Hz, 1H, Ar), 6.37 (d, J = 7.5 Hz, 1H, Ar); IR(KBr): 3502 cm^{-1} (OH-str), 3342 cm^{-1} (2°amine N–H Str), 3047 cm^{-1} (Ar CH str), 1660 cm^{-1} (C = N), 1614 cm^{-1}(Ar C = C), 1542 cm^{-1} (N–H Bend), 1301 cm^{-1} (C-N str), 1142 cm^{-1} (C-O str); ^{13}C NMR (125 MHz, DMSO d_6): δ 161.39, 161.07, 150.39, 147.65, 142.56, 141.52, 139.13, 137.86, 132.90, 132.14, 129.24, 128.73, 122.80, 121.38, 120.63, 115.48,

111.14, 108.12, 103.23; HREI-MS: m/z calcld for C$_{19}$H$_{14}$N$_4$O$_3$, [M]$^+$ 346.1066 Found 346.1044.

4.2.12. (E)-N'-(3,5-dihydroxybenzylidene)-9H-pyrido[3,4-b]indole-3-carbohydrazide (12)
^{1}H NMR (500 MHz, DMSO d_6): δ 12.06 (s, 1H, N–H), 12.01 (s, 1H, NH), 11.95 (s, 1H, OH), 9.52 (s, 1H, OH), 8.97 (s, 1H, H-C = N), 8.95 (s, 1H, pyrido-H), 8.51 (s, 1H, pyrido-H), 8.44 (d, J = 7.6 Hz, 1H, Ar), 7.67 (d, J = 7.6 Hz, 1H, Ar), 7.62 (d, J = 7.5 Hz, 1H, Ar), 7.31 (t, J = 7.8 Hz, 1H, Ar), 6.65–6.62 (m, 2H, Ar), 6.32 (dd, J = 7.2, 2.0 Hz, 1H, Ar); IR (KBr): 3305 cm^{-1} (OH-str), 3284 cm^{-1} (2° amine N–H Str), 3067 cm^{-1} (Ar CH str), 1620 cm^{-1} (C = O), 1580 cm^{-1} (N–H Bend),1150 cm^{-1} (C-O str); ^{13}C NMR (125 MHz, DMSO d_6): δ 161.59, 159.18, 156.3, 151.0, 148.87, 141.53, 139.40, 137.85, 136.76, 132.80, 129.25, 128.78, 122.85, 121.40, 120.63, 115.45, 112.80, 105.69, 104.86; HREI-MS: m/z calcld for C$_{19}$H$_{14}$N$_4$O$_3$, [M]$^+$ 346.1066 Found 346.1040.

4.2.13. (E)-N'-(3-methylbenzylidene)-9H-pyrido[3,4-b]indole-3-carbohydrazide (13)
^{1}H NMR (500 MHz, DMSO d_6): δ 12.04 (s, 1H, NH), 12.01 (s, 1H, NH), 8.96 (s, 1H, H-C = N), 8.94 (s, 1H, pyrido-H), 8.62 (s, 1H,

pyrido-H), 8.44 (d, J = 7.3 Hz, 1H, Ar), 7.68 (d, J = 7.5 Hz, 1H, Ar), 7.62 (dd, J = 7.0, 2.0 Hz, 1H, Ar), 7.51 (dd, J = 6.9, 2.0 Hz, 1H, Ar), 7.35–7.32 (m, 3H, Ar), 7.24 (d, J = 7.1 Hz, 1H, Ar), 2.41 (s, 3H, CH₃); IR υ (KBr disk): 3285 cm^{-1} (NH stretch), 3064 cm^{-1} (Ar.C–H stretch), 1649 cm^{-1} (C = O), 1537 cm^{-1} (C = N), 1363 cm^{-1} (C-N); ^{13}C NMR (125 MHz, DMSO d_6): δ 161.67, 148.57, 141.54, 139.38, 138.53, 137.86, 135.04, 132.80, 131.13, 129.25, 129.20, 128.78, 127.79, 124.99, 122.87, 121.41, 120.64, 115.50, 112.80, 21.57; HREI-MS: m/z calcld for C₂₀H₁₆N₄O, [M]$^+$ 328.1324 Found 328.1305.

4.2.14. (E)-N'-(4-methylbenzylidene)-9H-pyrido[3,4-b]indole-3-carbohydrazide (14)

^{1}H NMR (500 MHz, DMSO d_6): δ 12.01 (s, 1H, NH), 11.92 (s, 1H, NH), 8.94 (s, 1H, H-C = N), 8.92 (s, 1H, pyrido-H), 8.60 (s, 1H, pyrido-H), 8.44 (dd, J = 7.5 Hz, 1H, Ar), 7.81 (d, J = 7.9 Hz, 2H, Ar), 7.66–7.61 (m, 2H, Ar), 7.32 (d, J = 7.5 Hz, 1H, Ar-H), 7.25 (d, J = 7.9 Hz, 2H, Ar-H), 2.41 (s, 3H, CH₃); IR υ (KBr disk): 3290 cm^{-1} (NH stretch), 3050 cm^{-1} (Ar.C–H stretch), 1651 cm^{-1} (C = O), 1523 cm^{-1} (C = N), 1360 cm^{-1} (C-N); ^{13}C NMR (125 MHz, DMSO d_6): δ 161.59, 148.54, 141.54, 140.20, 139.43, 137.84, 132.79, 132.38, 129.91, 129.24, 128.78, 127.54, 122.87, 121.40, 120.63, 115.44, 112.79, 111.02, 107.29, 35.23; HREI-MS: m/z calcld for C₂₀H₁₆N₄O, [M]$^+$ 328.1324 Found 328.1307.

4.2.15. (E)-N'-(3-hydroxybenzylidene)-9H-pyrido[3,4-b]indole-3-carbohydrazide (15)

^{1}H NMR (500 MHz, DMSO d_6): δ 12.08 (s, 2H, 2xNH), 9.88 (s, 1H, OH), 9.03 (s, 1H, H-C = N), 8.94 (s, 1H, pyrido-H), 8.57 (s, 1H, pyrido-H), 8.45 (d, J = 7.4 Hz, 1H, Ar), 7.72 (d, J = 7.5 Hz, 1H, Ar), 7.62 (t, J = 7.2 Hz, 1H, Ar), 7.40 (t, J = 7.4 Hz, 1H, Ar), 7.34–7.30 (m, 3H, Ar), 6.82 (dd, J = 7.2, 2.0 Hz, 1H, Ar); IR (KBr): 3420 cm^{-1} (OH-str), 3205 cm^{-1} (2° amine N–H Str), 3032 cm^{-1} (Ar CH str), 1603 cm^{-1} (Ar C = C), 1503 cm^{-1} (N–H Bend), 1224 cm^{-1} (C-N str), 1160 cm^{-1} (C-O str); ^{13}C NMR (125 MHz, DMSO d_6): δ 161.64, 158.15, 148.58, 141.53, 139.38, 137.85, 136.35, 132.80, 130.34, 129.25, 128.78, 122.87, 121. 40, 120.64, 119.20, 117.76, 115.48, 113.17, 112.80; HREI-MS: m/z calcld for C₁₉H₁₄N₄O₂, [M]$^+$ 330.1117 Found 330.1097.

4.2.16. (E)-N'-(4-methoxybenzylidene)-9H-pyrido[3,4-b]indole-3-carbohydrazide (16)

^{1}H NMR (500 MHz, DMSO d_6): δ 12.05 (s, 1H, NH), 12.01 (s, 1H, NH), 9.01 (s, 1H, H-C = N), 8.95 (s, 1H, pyrido-H), 8.66 (s, 1H, pyrido-H), 8.47 (d, J = 7.5 Hz, 1H, Ar), 7.67 (d, J = 7.2 Hz, 1H, Ar), 7.62 (t, J = 6.9 Hz, 1H, Ar), 7.43–7.34 (m, 4H, Ar), 7.08 (dd, J = 7.0 2.0 Hz, 1H, Ar-H), 3.89 (s, 3H, OCH₃); IR υ cm^{-1} (KBr disk): 3309 cm^{-1} (NH stretch), 3070 cm^{-1} (Ar.C–H stretch), 1631 cm^{-1} (C = O), 1588 cm^{-1} (C = N), 1552 cm^{-1} (C-N), 1142 cm^{-1} (C-O str); ^{13}C NMR (125 MHz, DMSO d_6): δ 161.72, 160.04, 148.44, 141.55, 139.32, 137.88, 136.51, 132.85, 130.42, 129.25, 128.77, 122.86, 120.64, 120.58, 116.39, 116.60, 115.52, 112.81, 111.61, 55.66; HREI-MS: m/z calcld for C₂₀H₁₆N₄O₂, [M]$^+$ 344.1273 Found 344.1208.

4.3. Assay protocol for acetylcholinesterase and butyrylcholinesterase

The Ellman's method was used for the test substances to check their ability to inhibit AChE and BChE from electric eel and horse serum, respectively, as well as human cholinesterase (Sigma-Aldrich) (Ellman et al., 1961). The incubation of the test sample was done with 20 L of either the AChE/BChE solution or 140 L of sodium phosphate buffer (pH 8.0) for 15 min at room temperature.

AChE/BChE 10 μL and DTNB were used to start the reaction, respectively. 15 min later, unrestrained by the enzymatic hydrolysis of AChE and BChE, AChE or BChE was hydrolyzing the interaction of DTNB with thiocholine. Inhibition was estimated as a percentage (%) using the formula E - S / E 100, where E&S represent enzyme activity with and without the test material. Each sample's ChEs inhibitory activity was represented in terms of IC₅₀ value (g/mL) or μM necessary for the prevention of substrate hydrolysis (Mansha et al., 2021). The IC₅₀ values are determined for all substances using a general graph. Excel created the graph, and the IC₅₀ values were produced by considering that Y = 50 and identifying the value of × as the IC₅₀.

4.4. Molecular docking studies for acetylcholinesterase and butyrylcholinesterase

All compound structures were prepared using Chemdraw and minimized using CHARMM forcefield. The crystal structures of acetylcholinesterase (PDB: 4EY7) and butyrylcholinesterase (PDB: 1P0P) had been obtained from RCSB database and the structures were optimized using macromolecule module in Discovery Studio. Molecular docking studies had been validated and carried out using CDOCKER based on the coordinate of butyrylthiocholine within butyrylcholinesterase (x: 133.52, y: 115.38, z: 41.15) and donepezil within the active site of acetylcholinesterase (x: −14.10, y: −43.83, z: 27.66). The molecular docking results obtained were then analysed using Discovery Studio visualizer 2016.

4.5. Molecular dynamics for acetylcholinesterase and butyrylcholinesterase

Molecular dynamics for acetylcholinesterase and butyryl-cholinesterase had been performed using the results obtained from molecular docking studies. The selected protein–ligand complexes for acetylcholinesterase and butyrylcholinesterase were prepared and optimized using Protein Preparation Wizard in Maestro (Schrodinger Release 2019–3: Maestro, Schrodinger, LLC, New York, NY, USA 2017). The complexes were then solvated using water molecules (TIP3P) in an orthorhombic simulation box with a buffering distance of at least 10 Å. Sodium chloride (0.15 M) was added to achieve suitable physiological conditions. The OPLS_2005 force field was applied for the minimization of the solvated systems. Molecular dynamic simulation was then performed using Desmond V 5.9 package (Schrodinger 2019–3) accelerated by NVidia GTX3070 GPU. The total simulation time was set at 100 ns while time-step was set at 2 fs. The trajectories were recorded at 50 ps interval that generated 2000 frames. The molecular dynamic simulation was performed in the NPT ensemble by keeping the system temperature constant at 310 K using the NoseHoover chain thermostat, and the pressure constant at 1.01325 bar using the Martyna-Tobias-Klein barostat.

Declaration of competing interest

The authors declare that they have no known competing financial interests or personal relationships that could have appeared to influence the work reported in this paper.

References

Aaghaz, S., Sharma, K., Jain, R., Kamal, A., 2021. β-Carbolines as potential anticancer agents. Eur. J. Med. Chem. 216, 113321.

Ahmad, I., Fakhri, S., Khan, H., Jeandet, P., Aschner, M., Yu, Z.-L., 2020. Targeting cell cycle by β-carboline alkaloids in vitro: novel therapeutic prospects for the treatment of cancer. Chem.-Biol. Interact. 330, 109229.

Beus, M., Persoons, L., Daelemans, D., Schols, D., Savijoki, K., Varmanen, P., Yli-Kauhaluoma, J., Pavić, K., Zorc, B., 2022. Anthranilamides with quinoline and β-carboline scaffolds: design, synthesis, and biological activity. Mol. Divers., 1–18

Boccia, M., Di Vita, A., Diana, S., Margiotta, R., Imbriano, L., Rendace, L., Campanelli, A., D'Antonio, F., Trebbastoni, A., de Lena, C., 2019. Is losing one's way a sign of cognitive decay? Topographical memory deficit as an early marker of pathological aging. J. Alzheimer's Dis. 68 (2), 679–693.

Breijyeh, Z., Karaman, R., 2020. Comprehensive review on Alzheimer's disease: causes and treatment. Molecules 25 (24), 5789.

Downer, B., Al Snih, S., Chou, L.-N., Kuo, Y.-F., Raji, M., Markides, K.S., Ottenbacher, K. J., 2021. Changes in health care use by Mexican American Medicare beneficiaries before and after a diagnosis of dementia. J. Gerontol.: Series A 76 (3), 534–542.

Eichenbaum, H., 2017. Prefrontal–hippocampal interactions in episodic memory. Nat. Rev. Neurosci. 18 (9), 547–558.

Ellman, G.L., Courtney, K.D., Andres Jr, V., Featherstone, R.M., 1961. A new and rapid colorimetric determination of acetylcholinesterase activity. Biochem. Pharmacol. 7 (2), 88–95.

Gooyit, M., Tricoche, N., Javor, S., Lustigman, S., Janda, K.D., 2015. Exploiting the Polypharmacology of ß-Carbolines to Disrupt O. volvulus Molting. ACS Med. Chem. Lett. 6 (3), 339–343.

Hegazy, A., Mahmoud, S.H., Elshaier, Y.A., Shama, N.M.A., Nasr, N.F., Ali, M., El-Shazly, A.M., Mostafa, I., Mostafa, A., 2023. Antiviral activities of plant-derived indole and β-carboline alkaloids against human and avian influenza viruses. Sci. Rep. 13 (1), 1612.

Heo, J.H., Eom, B.H., Ryu, H.W., Kang, M.-G., Park, J.E., Kim, D.-Y., Kim, J.-H., Park, D., Oh, S.-R., Kim, H., 2020. Acetylcholinesterase and butyrylcholinesterase inhibitory activities of khellactone coumarin derivatives isolated from Peucedanum japonicum Thurnberg. Sci. Rep. 10 (1), 21695.

Huang, L.-K., Chao, S.-P., Hu, C.-J., 2020. Clinical trials of new drugs for Alzheimer disease. J. Biomed. Sci. 27 (1), 1–13.

Hussain, R., Rahim, F., Rehman, W., Taha, M., Khan, S., Zaman, K., Shah, A.A., Wadood, A., Imran, S., Abdellatif, M.H., 2022. Synthesis and molecular docking of new bis-thiazolidinone-based chalcone analogs as effective inhibitors of acetylcholinesterase and butyrylcholinesterase. Chem. Biodivers. 19 (10), e202200323.

Kamboj, A., Sihag, B., Brar, D.S., Kaur, A., Salunke, D.B., 2021. Structure activity relationship in β-carboline derived anti-malarial agents. Eur. J. Med. Chem. 221, 113536.

Kandiah, N., Pai, M.-C., Senanarong, V., Looi, I., Ampil, E., Park, K.W., Karanam, A.K., Christopher, S., 2017. Rivastigmine: the advantages of dual inhibition of acetylcholinesterase and butyrylcholinesterase and its role in subcortical vascular dementia and Parkinson's disease dementia. Clin. Interv. Aging, 697–707.

Khan, S., Ullah, H., Taha, M., Rahim, F., Sarfraz, M., Iqbal, R., Iqbal, N., Hussain, R., Ali Shah, S.A., Ayub, K., 2023. Synthesis, DFT studies, molecular docking and biological activity evaluation of thiazole-sulfonamide derivatives as potent Alzheimer's inhibitors. Molecules 28 (2), 559.

Khoury, R., Rajamanickam, J., Grossberg, G.T., 2018. An update on the safety of current therapies for Alzheimer's disease: focus on rivastigmine. Therap. Adv. Drug Safety 9 (3), 171–178.

Kontham, V., Ippakayala, B., Madhu, D., 2021. Synthesis of β-carboline fatty alcohol hybrid molecules and characterization of their biological and antioxidant activities. Arab. J. Chem. 14 (6), 103163.

Laine, A.E., Lood, C., Koskinen, A.M., 2014. Pharmacological importance of optically active tetrahydro-β-carbolines and synthetic approaches to create the C1 stereocenter. Molecules 19 (2), 1544–1567.

Mansha, M., Taha, M., Ullah, N., 2021. The design of fluoroquinolone-based cholinesterase inhibitors: Synthesis, biological evaluation and in silico docking studies. Arab. J. Chem. 14 (7), 103211.

Mascarenhas, A.M.S., de Almeida, R.B.M., de Araujo Neto, M.F., Mendes, G.O., da Cruz, J.N., Dos Santos, C.B.R., Botura, M.B., Leite, F.H.A., 2021. Pharmacophore-based virtual screening and molecular docking to identify promising dual inhibitors of human acetylcholinesterase and butyrylcholinesterase. J. Biomol. Struct. Dyn. 39 (16), 6021–6030.

Mathew, J., Ding, S., Kunz, K.A., Stacy, E.E., Butler, J.H., Haney, R.S., Merino, E.F., Butschek, G.J., Rizopoulos, Z., Totrov, M., 2022. Malaria Box-Inspired Discovery of N-Aminoalkyl-β-Carboline-3-Carboxamides, a Novel Orally Active Class of Antimalarials. ACS Med. Chem. Lett. 13 (3), 365–370.

Mushtaq, G., Greig, H.N., Khan, A.J., Kamal, A.M., 2014. Status of acetylcholinesterase and butyrylcholinesterase in Alzheimer's disease and type 2 diabetes mellitus. CNS Neurol. Disorders-Drug Targets (Formerly Current Drug Targets-CNS & Neurological Disorders) 13 (8), 1432–1439.

Nasr, T., Bondock, S., Youns, M., 2014. Anticancer activity of new coumarin substituted hydrazide–hydrazone derivatives. Eur. J. Med. Chem. 76, 539–548.

Obaid, R.J., Naeem, N., Mughal, E.U., Al-Rooqi, M.M., Sadiq, A., Jassas, R.S., Moussa, Z., Ahmed, S.A., 2022. Inhibitory potential of nitrogen, oxygen and sulfur containing heterocyclic scaffolds against acetylcholinesterase and butyrylcholinesterase. RSC Adv. 12 (31), 19764–19855.

Salgın-Gökşen, U., Gökhan-Kelekçi, N., Göktaş, Ö., Köysal, Y., Kılıç, E., Işık, Ş., Aktay, G., Özalp, M., 2007. 1-Acylthiosemicarbazides, 1, 2, 4-triazole-5 (4H)-thiones, 1, 3, 4-thiadiazoles and hydrazones containing 5-methyl-2-benzoxazolinones: synthesis, analgesic-anti-inflammatory and antimicrobial activities. Biorg. Med. Chem. 15 (17), 5738–5751.

Şenkardeş, S., Kaushik-Basu, N., Durmaz, I., Manvar, D., Basu, A., Atalay, R., Küçükgüzel, Ş.G., 2016. Synthesis of novel diflunisal hydrazide–hydrazones as anti-hepatitis C virus agents and hepatocellular carcinoma inhibitors. Eur. J. Med. Chem. 108, 301–308.

Settypalli, T., Chunduri, V.R., Maddineni, A.K., Begari, N., Allagadda, R., Kotha, P., Chippada, A.R., 2019. Design, synthesis, in silico docking studies and biological evaluation of novel quinoxaline-hydrazide hydrazone-1, 2, 3-triazole hybrids as α-glucosidase inhibitors and antioxidants. New J. Chem. 43 (38), 15435–15452.

Singh, D., Tiwari, S.K., Singh, V., 2019. A transition metal-free approach towards synthesis of β-carboline tethered 1, 3, 4-oxadiazoles via oxidative C-O bond formation. New J. Chem. 43 (1), 93–102.

Taha, M., Alshamrani, F.J., Rahim, F., Uddin, N., Chigurupati, S., Almandil, N.B., Farooq, R.K., Iqbal, N., Aldubayan, M., Venugopal, V., 2021a. Synthesis, characterization, biological evaluation, and kinetic study of indole base sulfonamide derivatives as acetylcholinesterase inhibitors in search of potent anti-Alzheimer agent. J. King Saud Univ.-Sci. 33 (3), 101401.

Taha, M., Rahim, F., Uddin, N., Khan, I.U., Iqbal, N., Salahuddin, M., Farooq, R.K., Gollapalli, M., Khan, K.M., Zafar, A., 2021b. Exploring indole-based-thiadiazole derivatives as potent acetylcholinesterase and butyrylcholinesterase enzyme inhibitors. Int. J. Biol. Macromol. 188, 1025–1036.

Torromino, G., Maggi, A., De Leonibus, E., 2021. Estrogen-dependent hippocampal wiring as a risk factor for age-related dementia in women. Prog. Neurobiol. 197, 101895.

Wu, J., Pistolozzi, M., Liu, S., Tan, W., 2020. Design, synthesis and biological evaluation of novel carbamates as potential inhibitors of acetylcholinesterase and butyrylcholinesterase. Biorg. Med. Chem. 28 (5), 115324.

Zhu, Y., Zhao, J., Luo, L., Gao, Y., Bao, H., Li, P., Zhang, H., 2021. Research progress of indole compounds with potential antidiabetic activity. Eur. J. Med. Chem. 223, 113665.